Solar Energy 163 (2018) 591–599

Contents lists available at ScienceDirect

Solar Energy

journal homepage: www.elsevier.com/locate/solener

Optimization of solar photovoltaic system integrated with phase change material

Sourav Khanna[a,*], K.S. Reddy[b], Tapas K. Mallick[a,*]

[a] Environment and Sustainability Institute, Penryn Campus, University of Exeter, Cornwall TR10 9FE, United Kingdom
[b] Heat Transfer and Thermal Power Laboratory, Department of Mechanical Engineering, Indian Institute of Technology Madras, Chennai 600 036, India

ARTICLE INFO

Keywords:
Phase change material
Solar photovoltaic
Thermal management
Optimization

ABSTRACT

The rise in the temperature of photovoltaic (PV) leads to decrease in the solar to electricity conversion efficiency. This paper presents a simulated study to investigate the thermal management of the PV panel using phase change material (PCM). It is found that once the PCM is fully melted, the rate of heat extraction by PCM decreases and, thus, the PV temperature starts increasing rapidly. In literature, the studies related to the performance analysis of the PV-PCM system are available. However, the optimization of the PCM quantity to cool the PV in various operating conditions and solar radiation levels is not available. Thus, it has been carried out in the presented work. The effects of the operating conditions (wind azimuth angle i.e. wind direction, wind velocity, melting temperature of PCM and ambient temperature) on the optimum depth of the PCM container have been analysed. The results show that as wind azimuth angle increases from 0° to 90°, the optimum depth of the PCM container (to maintain the PV at lower temperature) increases from 3.9 cm to 5.3 cm for ΣI_T = 5 kWh/m^2/day and from 2.4 cm to 3.2 cm for ΣI_T = 3 kWh/m^2/day for the chosen parameters.

1. Introduction

The temperature of the photovoltaic (PV) cell rises during its operation which reduces its solar to electricity conversion efficiency (Khanna et al., 2017a). The studies that analyse the thermal management of the PV by extracting the heat using phase change material (PCM) have been reviewed. Some studies have been reported that carried out the experimental analysis which are as follows: Huang et al. (2006a) have investigated the performance of the PV-PCM (mimicked PV) system for two cases (with and without fins). It has beenfound that the temperature rise of the front surface can be reduced by 10 °C using fins at an insolation of 750 W/m^2 and an ambient temperature of 23 °C. Straight fins, wire matrix and strip matrix are used to enhance the heat transfer. Hasan et al. (2015) have analysed the PV-PCM system under two different weather conditions (Dublin and Vehari) and found that for Dublin, the maximum temperature reduction in PV is 10 °C at an insolation of 970 W/m^2 and an ambient temperature of 24 °C and for Vehari, it is 21.5 °C at an insolation of 950 W/m^2 and an ambient temperature of 32 °C. Researchers have used different types of PCMs. A yellow petroleum jelly has been proposed by Indartono et al. (2014) and a decrease in the PV temperature from 60 °C to 54.3 °C has been reported for a PV-on-roof system at an insolation of 1120 W/m^2 and an ambient temperature of 25 °C and from 44.8 °C to 42.2 °C for PV-on-stand system. Hasan et al. (2010) have analysed five different PCMs. At solar flux of 1000 W/m^2 and an ambient temperature of 20 °C, a maximum reduction of 18 °C in the PV temperature has been reported. Sharma et al. (2016) have coupled the PCM with a building integrated concentrated PV (BICPV) which resulted in increase of 1.15%, 4.20% and 7.7% in the electrical efficiency at insolation of 500 W/m^2, 750 W/m^2 and 1000 W/m^2 respectively. Huang et al. (2011) have reported the crystalline segregation of the PCM. It has been concluded that the deployment of the internal fins enhances the system's performance. Waksol A, RT27 and RT35 are used for the study at an insolation of 750 W/m^2 and an ambient temperature of 19 °C. Browne et al. (2015b, 2016) have used a pipe network inside the PCM container to utilize the stored heat by flowing water through the pipes which has led to a thermal efficiency of 20–25% at Dublin for three consecutive days in July having an insolation of 950 W/m^2 and an ambient temperature of 20 °C around noon. An increase of 6 °C in the water temperature has been reported against the case when the PV-Thermal system is used without PCM. Some review studies (Du et al., 2013; Browne et al., 2015a; Ma et al., 2015; Shukla et al., 2017) are also reported focusing the thermal performance of the PV-PCM system.

Apart from the experimental studies, there have been several numerical studies for one, two and three-dimensional thermal analysis of the PV-PCM system. The following investigations have carried out the

* Corresponding authors.
E-mail addresses: s.khanna@exeter.ac.uk (S. Khanna), t.k.mallick@exeter.ac.uk (T.K. Mallick).

https://doi.org/10.1016/j.solener.2018.01.002
Received 16 March 2017; Received in revised form 15 December 2017; Accepted 1 January 2018
Available online 13 March 2018

Nomenclature

a_i	coefficient appeared in Eq. (29)
B	liquid fraction of PCM
C_p	specific heat capacity (J/kg K)
D	Dirac delta function
F	view factor between surfaces
g	acceleration due to gravity (m^2/s)
G	heat generation (W/m^3)
Gr	Grashof number
h	convective heat transfer coefficient (W/m^2 K)
I_T	solar radiation on tilted surface (W/m^2)
k	thermal conductivity (W/m K)
L	length of the system (m)
L_{ch}	characteristic length (m)
L_h	latent heat (J/kg)
p	pressure (Pa)
Pr	Prandtl number of air
Q_L	rate of heat loss from the top surface (W/m^2)
Re	Reynolds number
S_h	solar radiation converted into heat in the system (W/m^2)
t	time (s)
T	temperature (K)
T_m	peak melting temperature of PCM (K)
u	velocity of melted PCM (m/s)
v_w	wind velocity (m/s)

Greek symbols

β	tilt angle of the panel (rad)
β_c	thermal expansion coefficient of PCM (/K)
γ	wind azimuth angle i.e. the angle made by wind stream with the projection of surface normal on horizontal plane (rad)
δ	depth of PCM container (m)
ΔT	phase change zone (K)
ε	emissivity for long wavelength radiation
$\eta_{PV\ module}$	solar radiation to electricity conversion efficiency of PV module
μ	dynamic viscosity of air (kg/ms)
ν	kinematic viscosity of air (m^2/s)
ρ	density (kg/m^3)
ρ_{PV}	reflectivity of the top surface of the PV module
σ	Stefan–Boltzmann constant ($W/m^2 K^4$)

Abbreviation

BICPV	building integrated concentrated PV
EVA	ethylene vinyl acetate
PCM	phase change material
PV	photovoltaic

Subscripts

a	ambient
c	critical
for	forced convection
g	ground
l	liquid phase
nat	natural convection
P	PCM
s	sky; solid phase
t	top surface
x	x direction
y	y direction

one-dimensional analysis considering the conductive energy flow alone inside the PCM. Brano et al. (2014) have reported a finite difference method for analysing the PV-PCM system which maintains the relative average mismatch between the calculated and the measured values of the PV temperature below 7% for summers in Palermo having an insolation of 1000 W/m^2 and an ambient temperature of 25 °C around noon. Atkin and Farid (2015) have analysed four systems: (A) only-PV, (B) PV-PCM, (C) PV-Heatsink and (D) PV-PCM-Heatsink and found an electricity enhancement of 7.32%, 11.70% and 12.97% using systems B, C and D respectively as compared to system A. Smith et al. (2014) have calculated the electricity generation by PV-PCM system for countries all over the world and the performance in the tropical regions are found to be the best. An increase of over 6% in the electricity output has been reported for Mexico and Eastern Africa. Mahamudul et al. (2016) have studied the behaviour of the PV-PCM system and found a reduction of 10 °C in the PV temperature for a period of 6 h using RT 35 PCM under Malaysian climate having maximum insolation of 1000 W/m^2 and an ambient temperature of 35 °C. Kibria et al. (2016) have analysed three different PCMs and found a 5% increment in the PV efficiency at an insolation of 750 W/m^2 and an ambient temperature of 20 °C. It is also found that for 8 h of operation, RT20 gets fully melted whereas RT25 and RT28HC gets melted up to 80% and 65% respectively. Park et al. (2014) have studied the performance of the PV-PCM system by varying the melting temperature and the thickness of the PCM layer. It is found that the PV temperature can be reduced by 10 °C using 100 mm thick PCM layer at an insolation of 780 W/m^2 and an ambient temperature of 19 °C. Aelenei et al. (2014) have achieved a thermal efficiency of 10% and an overall (electrical + thermal) efficiency of 20% in a building integrated PV-PCM system at Lisbon for a day having an insolation of around 900 W/m^2 and an ambient temperature of 12 °C at noon. Elarga et al. (2016) have analysed the performance of the PV-PCM system integrated in double skin facades and found a reduction of 20–30% in the monthly energy demand for cooling and an increment of 5–8% in the electricity generation. The locations considered for the study are Venice, Helsinki and Abu Dhabi. The reduction in the heating load in cold-dominated locations is found to be limited.

Despite above studies, it is a fact that the energy flow due to convection inside the melted PCM affects the system's performance significantly (Kant et al., 2016). The following numerical studies have considered it and the side walls of the PCM container are considered to be insulated which leads to the temperature variations along the height and the thickness of the system. Thus, the following studies have carried out the two-dimensional thermal analysis. Huang et al. (2004) have studied the PV-PCM (mimicked PV) system with and without fins at an insolation of 1000 W/m^2 and an ambient temperature of 20 °C. The temperature of the front surface of the system has been reported to be reduced by 3 °C using fins. It is found that the PCM (melting temperature 32 °C) container having depth of 20 mm can maintain the front surface temperature under 36.4 °C for 80 min. Ho et al. (2012) have reported an increase in the PV electrical efficiency from 19.1% to 19.5% at an insolation of 650 W/m^2 and an ambient temperature of 30 °C and from 17.86% to 17.99% at an insolation of 450 W/m^2 and an ambient temperature of 20 °C using the microencapsulated PCM having melting temperature of 26 °C and depth to length ratio of PCM container as 0.277. Huang (2011) has studied the use of two different PCMs in a same container at an insolation of 1000 W/m^2 and an ambient temperature of 20 °C. RT27-RT27, RT27-RT21 and RT31-RT27 PCMs have been chosen and RT27-RT21 combination is found to be the best. Khanna et al. (2017b) have studied the effect of tilt angle of the PV-PCM system on the melting rate of the PCM and found that as tilt

increases, melting rate increases. The simulations are performed at an insolation of 1000 W/m^2. Emam et al. (2017) have analysed the effect of the inclination on the performance of the concentrated PV-PCM system and found that 45° tilt angle is the best for the reduction in PV temperature. The simulations are performed at insolation of 5000 W/m^2 and 20,000 W/m^2 and an ambient temperature of 25 °C. During phase change, the thermal properties of the PCM vary rapidly and Biwole et al. (2013) have deployed a Dirac delta function to model the same for the convergence of the solution.

The heat losses from the side walls of the PCM container have been considered by Huang et al. (2006b, 2007) thereby conducting the three-dimensional thermal analysis of the PV-PCM system. It is concluded that the two-dimensional analysis itself can predict the results to a fair amount of accuracy. The mismatch is reported as 2 °C at an insolation of 750 W/m^2 and an ambient temperature of 20 °C. Ho et al. (2014, 2015) have presented the three-dimensional thermal model without considering the convective energy flow inside the PCM and found an increment of 2.1% in the electricity generation for southern-Taiwan climate. The PCM having melting temperatures 17 °C, 18 °C and 30 °C are considered for the simulations.

From the reviewed literature, it has been found that once the PCM is fully melted, the PV temperature starts increasing rapidly (Huang et al., 2004, 2006a, 2006b, 2007, 2011; Huang, 2011; Biwole et al., 2013; Emam et al., 2017; Khanna et al., 2017b). The optimization of the PCM's quantity to cool the PV in various operating conditions and solar radiation levels is thus the focus of the presented work which has not yet been reported in the literature by any researcher.

2. Methodology

A PV panel with a PCM container attached at its rear was considered for the presented study as shown in Fig. 1 with β as its tilt angle. The PV panel consisted of five layers. The depth and the length of the PCM container were denoted by δ and L respectively. The side walls and the bottom were thermally insulated so that the only relevant thermal variations occurred along the thickness (y direction) and the length of the system (x direction). It is observed that when the PCM starts melting, the solid portion tends to get displaced downwards pushing the melted one upwards resulting in a temperature gradient along the height inside the container leading to a non-uniform PV temperature which hampers the PV performance. Thus, a highly conductive (aluminium) layer was introduced behind the PV. It was found that for L = 1 m, the temperature gradient reached to 15 °C. However, by attaching shorter PCM containers having length (L) 25 cm, the non-uniformity in the PV temperature reduced to 4 °C.

The study was carried out based on the following assumptions

(i) The solar flux incident on the surface of the PV was considered to be uniformly distributed. It means that the non-uniformity created by the localised dirt on the PV and clouds was not considered.
(ii) The PV was taken as isotropic and homogenous.
(iii) The effects of the temperature and the incident solar radiation on the PV performance were incorporated as variations in the solar to electricity conversion efficiency of the PV.
(iv) The variations in the thermal properties of the PV material with temperature were neglected.
(v) The bottom and the side walls were insulated hence the heat losses from the same were neglected.
(vi) The effect of the interfacial resistances on the thermal performance of the system were neglected.
(vii) To keep the model simple, all the heat was considered to be generated in the silicon layer.
(viii) The properties of the PCM in solid and liquid phases were homogeneous and isotropic.
(ix) The variations in the thermal properties of the PCM with change in temperature were neglected within same phase.
(x) The flow inside the melted PCM was considered to be laminar and incompressible.

Out of the total solar radiation incident on the surface of the PV (I_T), a fraction ($\rho_{PV} I_T$) was lost due to reflection and the rest got absorbed by the system which can be written as $(1-\rho_{PV}) \times I_T$ where ρ_{PV} is the reflectivity of the top surface of the PV module. A portion of the absorbed radiation was utilised in producing electricity and the rest got converted into heat (S_h) which can be written as follows:

$$S_h = (1-\rho_{PV})I_T - \eta_{PV\ module} I_T \tag{1}$$

where $\eta_{PV\ module}$ is the solar radiation to electricity conversion efficiency of the PV module. A part of the generated heat got dissipated to surroundings via convection and radiation from the panel's top which can be given as follows:

$$Q_L = h[T_{at\ y=0} - T_a] + \sigma\varepsilon_t F_{ts}[T^4_{at\ y=0} - T^4_s] + \sigma\varepsilon_t F_{tg}[T^4_{at\ y=0} - T^4_g] \tag{2}$$

where h is the convective heat transfer coefficient (combination of natural and forced convection) between the top surface and the ambient, T_a is the ambient temperature, σ is the Stefan–Boltzmann constant, ε_t is the emissivity of the top surface for long wavelength radiation, $F_{t,s}$ and $F_{t,g}$ are the respective view factors of the top surface to sky and ground. T_s and T_g are the sky and ground temperatures respectively. Kaplani and Kaplanis (2014) had presented an expression for h which can be given as follows:

$$h = \begin{cases} h_{for}; & if\ Gr/Re^2 \leqslant 0.01 \\ |h^{7/2}_{nat} + h^{7/2}_{for}|^{2/7}; & if\ 0.01 < Gr/Re^2 < 100, \beta = 0° \\ |h^{3}_{nat} + h^{3}_{for}|^{1/3}; & if\ 0.01 < Gr/Re^2 < 100, \beta > 0° \\ h_{nat}; & if\ Gr/Re^2 \geqslant 100 \end{cases} \tag{3}$$

where Gr (Kaplani and Kaplanis, 2014) and Re (Kaplani and Kaplanis, 2014) are the Grashof and Reynolds numbers respectively. h_{nat} and h_{for} are the heat transfer coefficients of the top surface for natural and forced convection respectively and can be given as follows (Kaplani and Kaplanis, 2014):

$$h_{nat} = \begin{cases} \left[\begin{matrix} 0.13\{(GrPr)^{1/3} - (Gr_c Pr)^{1/3}\} + \\ 0.56(Gr_c Pr\ \sin\beta)^{1/4} \end{matrix}\right] k_a/L_{ch} & if\ \beta > 30° \\ [0.13(GrPr)^{1/3}]k_a/L_{ch} & if\ \beta \leqslant 30° \end{cases} \tag{4}$$

$$h_{for} = 0.848 k_a\ [\sin\beta \cos\gamma\ v_w\ Pr/\nu]^{0.5} (L_{ch}/2)^{-0.5} \tag{5}$$

where Pr is the Prandtl number of the air, Gr_c is the critical Grashof number ($=1.327 \times 10^{10}\ \exp\{-3.708(\pi/2 - \beta)\}$), k_a is the thermal conductivity of the air, L_{ch} is the characteristic length (the length of the surface along the direction of the air flow), γ is the wind azimuth angle

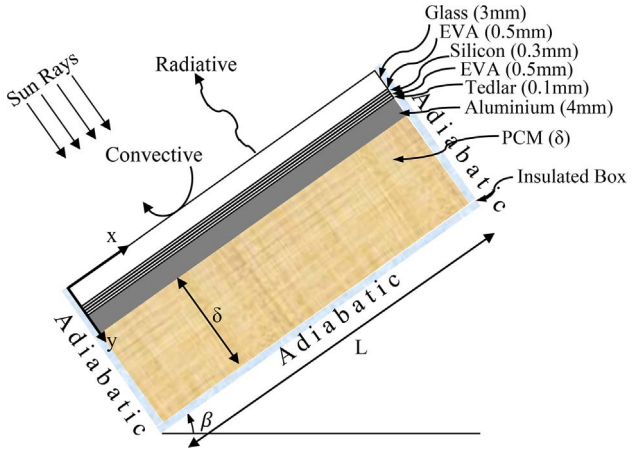

Fig. 1. System chosen for the current study.

(the angle made between the wind stream and the projection of PV's surface normal on the horizontal plane), v_w is the wind velocity and ν is the kinematic viscosity of the air.

The governing equations for the PV-PCM system are described in the subsequent sub-sections.

2.1. Solid portions

The temperature of the i^{th} layer of the solid portions of the system in x and y directions at any instant t was calculated by solving the following equation:

$$\rho_i C_{p,i} \frac{\partial T_i}{\partial t} = G_i + k_i \left(\frac{\partial^2 T_i}{\partial x^2} + \frac{\partial^2 T_i}{\partial y^2} \right) \tag{6}$$

where ρ_i, $C_{p,i}$, T_i, G_i and k_i are the density, specific heat capacity, temperature, heat generation (i.e. the fraction of the solar radiation converted into heat) and thermal conductivity of the i^{th} layer respectively. The boundary conditions for the above equation were as follows:

(a) The rate of heat loss from the side walls was 0 because of perfect insulation. It can be expressed mathematically in following manner:

$$k_i \frac{\partial T_i}{\partial x}_{at\ x=0} = k_i \frac{\partial T_i}{\partial x}_{at\ x=L} = 0 \tag{7}$$

(b) The rate of heat entering the i^{th} layer from its bottom surface was equal to the rate of heat leaving the $(i+1)^{th}$ layer from its top surface:

$$k_i \frac{\partial T_i}{\partial y} = k_{i+1} \frac{\partial T_{i+1}}{\partial y} \ at\ interface\ of\ i^{th}\ and\ (i+1)^{th}\ layer \tag{8}$$

(c) The rate of heat dissipated from the top surface of the 1st layer was equal to the rate of heat loss (convective and radiative) from the same surface:

$$k_1 \frac{\partial T_1}{\partial y}_{at\ y=0} = Q_L \tag{9}$$

(d) The temperature of the ith layer was equal to the ambient at $t = 0$ s:

$$T_i = T_a\ at\ t = 0 \tag{10}$$

2.2. PCM

In order to calculate the temperature of the PCM and the velocities of the melted PCM in x and y directions at any time t, the following equations were solved:

$$\rho_P C_{p,P} \frac{\partial T_P}{\partial t} = \frac{\partial}{\partial x}\left(k_P \frac{\partial T_P}{\partial x} - \rho_P C_{p,P} u_x T_P \right) + \frac{\partial}{\partial y}\left(k_P \frac{\partial T_P}{\partial y} - \rho_P C_{p,P} u_y T_P \right) \tag{11}$$

$$\rho_P \left(\frac{\partial u_x}{\partial t} + u_x \frac{\partial u_x}{\partial x} + u_y \frac{\partial u_x}{\partial y} \right) = -\frac{\partial p}{\partial x} + \mu(T) \left(\frac{\partial^2 u_x}{\partial x^2} + \frac{\partial^2 u_x}{\partial y^2} \right) + F_{bx} \tag{12}$$

$$\rho_P \left(\frac{\partial u_y}{\partial t} + u_x \frac{\partial u_y}{\partial x} + u_y \frac{\partial u_y}{\partial y} \right) = -\frac{\partial p}{\partial y} + \mu(T) \left(\frac{\partial^2 u_y}{\partial x^2} + \frac{\partial^2 u_y}{\partial y^2} \right) + F_{by} \tag{13}$$

$$\frac{\partial u_x}{\partial x} + \frac{\partial u_y}{\partial y} = 0 \tag{14}$$

where ρ_P, $C_{p,P}$, T_P and k_P are the density, specific heat capacity, temperature and thermal conductivity of the PCM respectively. u_x and u_y are the velocities of the melted PCM in x and y directions respectively, p is the pressure and μ is the dynamic viscosity. F_{bx} and F_{by} represent the buoyancy forces in x and y directions respectively. The boundary conditions for the above equations were as follows:

(a) The rate of heat loss from the bottom was 0 because of the perfect insulation. It can be expressed mathematically as follows:

$$k_P \frac{\partial T_P}{\partial y} = 0\ at\ bottom\ wall \tag{15}$$

(b) The rate of heat loss from the side walls was 0:

$$k_P \frac{\partial T_P}{\partial x}_{at\ x=0} = k_P \frac{\partial T_P}{\partial x}_{at\ x=L} = 0 \tag{16}$$

(c) The temperature of the PCM was equal to the ambient temperature at $t = 0$ s:

$$T_P = T_a\ at\ t = 0 \tag{17}$$

(d) The velocities of the melted PCM in x and y directions were 0 m/s at all four inner walls of the PCM container:

$$u_x = u_y = 0\ at\ all\ \ inner\ walls\ of\ PCM\ container \tag{18}$$

(e) The velocities were also 0 m/s at t = 0 s:

$$u_x = u_y = 0\ at\ t = 0 \tag{19}$$

In Eqs. (12) and (13), F_{bx} and F_{by} represented the buoyancy forces which can be given as follows:

$$F_{bx} = \rho g_x = \rho_l [1 - \beta_c (T_P - T_m)] g_x \tag{20}$$

$$F_{by} = \rho g_y = \rho_l [1 - \beta_c (T_P - T_m)] g_y \tag{21}$$

where g_x and g_y are the accelerations due to gravity in x and y directions respectively. ρ_l is the density of the PCM when it is in liquid phase. β_c and T_m are the thermal expansion coefficient and the peak melting temperature of the PCM respectively.

Since the properties of the PCM vary with the change in phase, they were considered as a function of temperature. Following the study presented by Biwole et al. (2013), the variation in $C_{p,P}$ with temperature can be given as follows:

$$C_{p,P}(T) = \begin{cases} C_{ps} & if\ \ T < (T_m - \Delta T/2) \\ C_{ps} + (C_{pl} - C_{ps})B + L_h D & if\ \ T_m - \Delta T/2 \leqslant T \leqslant T_m + \Delta T/2 \\ C_{pl} & if\ \ T > (T_m + \Delta T/2) \end{cases} \tag{22}$$

where C_{ps} and C_{pl} are the specific heat capacities of the PCM when it is in solid and liquid phases respectively. L_h is the latent heat capacity of the PCM. ΔT is the temperature's phase change zone which lies between solidification temperature ($T_m - \Delta T/2$) and liquidification temperature ($T_m + \Delta T/2$). Solidification temperature is the one below which the PCM is fully solid and liquidification temperature is the one above which the PCM is fully liquid. In between these temperature points, the PCM changes its phase. While changing the phase, the fraction of liquid phase is defined as liquid fraction of the PCM and can be given as follows:

$$B(T) = \begin{cases} 0 & if\ \ T < (T_m - \Delta T/2) \\ \frac{T - (T_m - \Delta T/2)}{\Delta T} & if\ \ T_m - \Delta T/2 \leqslant T \leqslant T_m + \Delta T/2 \\ 1 & if\ \ T > (T_m + \Delta T/2) \end{cases} \tag{23}$$

D (in Eq. (22)) is the Dirac delta function which takes care of the abrupt nature of the variation in the specific heat capacity during phase change. It is equal to 0 everywhere except for the phase change region where it can be given as follows:

$$D(T) = \frac{e^{-(T-T_m)^2/(\Delta T/4)^2}}{\sqrt{\pi(\Delta T/4)^2}} \tag{24}$$

Similarly, the variations in the ρ_P and k_P with temperature can be given as follows:

$$\rho_P(T) = \begin{cases} \rho_s & if\ T < (T_m - \Delta T/2) \\ \rho_s + (\rho_l - \rho_s)B(T) & if\ T_m - \Delta T/2 \leqslant T \leqslant T_m + \Delta T/2 \\ \rho_l & if\ T > (T_m + \Delta T/2) \end{cases} \tag{25}$$

$$k_P(T) = \begin{cases} k_s & if\ T < (T_m - \Delta T/2) \\ k_s + (k_l - k_s)B(T) & if\ T_m - \Delta T/2 \leqslant T \leqslant T_m + \Delta T/2 \\ k_l & if\ T > (T_m + \Delta T/2) \end{cases} \tag{26}$$

where ρ_s, ρ_l, k_s and k_l are the densities and the thermal conductivities of the PCM when it is in solid and liquid phases respectively. The variation in the viscosity of the PCM with temperature was incorporated as follows (Biwole et al., 2013):

$$\mu(T) = \mu_l[1 + A(T)] \tag{27}$$

where

$$A(T) = \frac{10^5\{1 - B(T)\}^2}{B(T)^3 + 10^{-3}} \tag{28}$$

The above Eqs. (27) and (28) ensured that for the portion of the PCM where temperature was less than the solidification temperature ($T_m - \Delta T/2$), a very high viscosity was taken and the portion of the PCM where temperature was above liquidification temperature ($T_m + \Delta T/2$), a very low viscosity was taken.

Due to the issues related to the convergence, the sharp variations in the thermal properties of the PCM during phase change must be handled delicately. For this, Biwole et al. (2013) proposed a second order continuous differentiable function for the liquid fraction of PCM (B) as follows:

$$B(T) = \sum_{i=0}^{6} a_i T^i \tag{29}$$

$$\mathrm{B}_{\mathrm{Tm}-\frac{\Delta T}{2}} = \frac{\mathrm{dB}}{\mathrm{dT}}_{\mathrm{Tm}-\frac{\Delta T}{2}} = \frac{\mathrm{d^2B}}{\mathrm{dT^2}}_{\mathrm{Tm}-\frac{\Delta T}{2}} = \frac{\mathrm{dB}}{\mathrm{dT}}_{\mathrm{Tm}+\frac{\Delta T}{2}} = \frac{\mathrm{d^2B}}{\mathrm{dT^2}}_{\mathrm{Tm}+\frac{\Delta T}{2}} = 0$$
$$\mathrm{B}_{\mathrm{Tm}+\frac{\Delta T}{2}} = 1\ and\ \mathrm{B}_{\mathrm{Tm}} = \frac{1}{2} \tag{30}$$

The coefficients (a_i) appeared in Eq. (29) were calculated using the above conditions (Eq. (30)) and can be given as follows:

$$\begin{bmatrix} a_0 \\ a_1 \\ a_2 \\ a_3 \\ a_4 \\ a_5 \\ a_6 \end{bmatrix} = \begin{bmatrix} 1 & b & b^2 & b^3 & b^4 & b^5 & b^6 \\ 0 & 1 & 2b & 3b^2 & 4b^3 & 5b^4 & 6b^5 \\ 0 & 0 & 2 & 6b & 12b^2 & 20b^3 & 30b^4 \\ 0 & 1 & 2c & 3c^2 & 4c^3 & 5c^4 & 6c^5 \\ 0 & 0 & 2 & 6c & 12c^2 & 20c^3 & 30c^4 \\ 1 & c & c^2 & c^3 & c^4 & c^5 & c^6 \\ 1 & d & d^2 & d^3 & d^4 & d^5 & d^6 \end{bmatrix}^{-1} \begin{bmatrix} 0 \\ 0 \\ 0 \\ 0 \\ 0 \\ 1 \\ 0.5 \end{bmatrix} \tag{31}$$

where $b = T_m - \Delta T/2$, $c = T_m + \Delta T/2$ and $d = T_m$.

3. Solution method

Using ANSYS Fluent 17.1, the geometry of the PV-PCM system was constructed by generating separate bodies for Glass, EVA, Silicon, EVA, Tedlar, Aluminium and PCM layers. The mesh was generated using a quadrilateral grid. The mesh interfaces between different layers of the system were formed and coupled appropriately. The mesh size (i.e. the distance between the successive nodes of the grid) was chosen as 1 mm as it was found that the decrease in the mesh size from 2 mm to 1 mm and from 1 mm to 0.5 mm changed the results by ±1.5 °C and ±0.2 °C respectively. The boundary conditions were applied on each wall of the geometry. The Pressure-Velocity coupling SIMPLE scheme was used for solving the equations. The iterations were allowed to continue until the values of the energy, velocity and continuity residuals reached to 10^{-8}, 10^{-4} and 10^{-4} respectively beyond which, no further significant improvement was observed in the results.

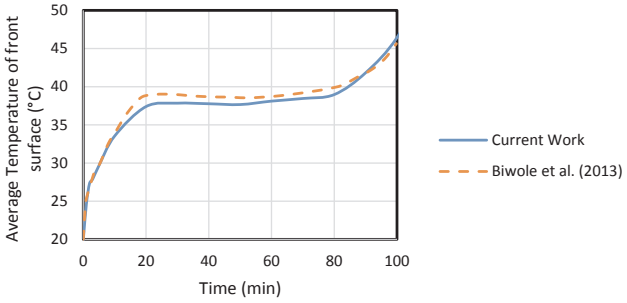

Fig. 2. Variations in the average temperature of the front surface of vertical system with time.

4. Validation

Thermal performance of the PCM in a vertical aluminium box had been investigated numerically by Biwole et al. (2013) for RT 25 HC PCM. The length (L) and the depth (δ) of the PCM container were taken as 132 mm and 20 mm respectively. The thicknesses of the aluminium plates at front and rear of the PCM layer had been kept as 4 mm. The incident solar radiation (I_T) and the ambient temperature (T_a) were chosen to be 1000 W/m^2 and 20 °C respectively. The overall heat loss coefficients from front and back of the system were taken as 10 W/m^2 K and 5 W/m^2 K respectively. The other outer walls of the system were considered as insulated with nil heat loss coefficients. They had reported the variation in the temperature of the front surface of the system with time. To validate the model of the presented work, the equations were solved by taking same parameters as those of Biwole et al. (2013). The variation in the front surface temperature with time has been plotted in Fig. 2 along with their values. The calculations suggest that the results differ from the original work within the range of ±1.5 °C. The results also show that beyond t = 20 min, the temperature stabilizes and after t = 80 min, it again starts increasing. The same trend had been reported by Biwole et al. (2013).

Huang et al. (2007) had experimentally studied the thermal performance of the PCM in a vertical aluminium box with RT 25 HC PCM. The length (L) and the depth (δ) of the PCM container were taken as 40 mm and 20 mm respectively. The thicknesses of the aluminium plates at front and back of the PCM layer had been taken as 5 mm. The incident radiation (I_T) and the ambient temperature (T_a) were 750 W/m^2 and 20 °C respectively. The front and back of the system were not insulated while the other outer walls were. They had reported the variation in the temperature of the front surface of the system with time. To validate the model of the presented work with the experimental one, the calculations had been carried out by taking similar parameters. The variation in the front surface temperature with time has been plotted in Fig. 3 along with the experimentally measured values. The results differ from the original work within the range of −2.0 °C to +0.7 °C. It is also observed that the temperature is stabilized from t = 17 min to t = 60 min, beyond which, it again starts going up. The same trend had been reported by Huang et al. (2007).

5. Results and discussion

For the presented work, the variations in the temperature of the PV-PCM system with time had been computed for various depths of the PCM container. The optimum depth had been calculated to keep the PV cool during the operation for various daily solar radiation levels. The effect of operating conditions on the optimum depth had also been investigated and is presented in Sections 5.1–5.4. The values of the

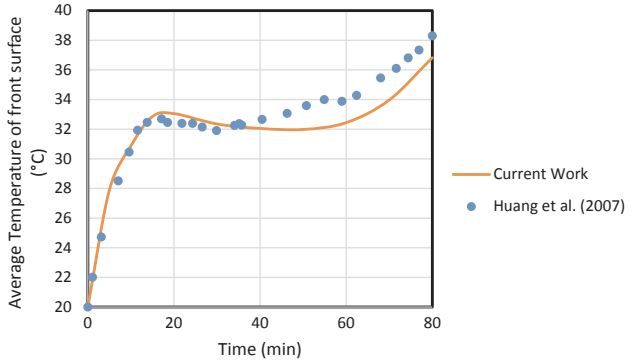

Fig. 3. Comparison of the values calculated using current work with the measured ones.

Table 1
Thermo-physical properties of PV and aluminium layer.

	Glass	EVA	Silicon	Tedlar	Aluminium
C_p (J/kg K)	500	2090	677	1250	903
k (W/m K)	1.8	0.35	148	0.2	211
Length (cm)	25	25	25	25	25
Thickness (mm)	4	0.5	0.3	0.1	4
ρ (kg/m^3)	3000	960	2330	1200	2675

parameters used for the calculations are presented in Tables 1 and 2. Huang et al. (2006a) had concluded that the Solid-Liquid PCM was more effective in PV's cooling as compared to the Solid-Solid PCM. Thus, the same had been chosen for the presented study.

The variations in the temperature of the PV with time have been presented in Fig. 4 for various depths of PCM container. The results show that the PV temperature shoots up initially and then gradually stabilises. It again starts increasing beyond a point and accelerates. It can be explained in following manner. Initially, the PCM in the container was in solid phase and its rate of heat extraction was very less due to low thermal conductivity. Later on, the PCM started melting and extracting heat (latent) from the PV without rise in temperature. At a point, the PCM got almost fully melted where it had absorbed all the latent heat. It resulted in lower rate of heat extraction by the PCM (only sensible) and, thus, the PV temperature started shooting up at faster rate.

The results also show that the increment in the depth of the PCM container leads to increase in the cooling capacity in terms of duration. However, for a fixed total daily solar radiation, beyond a certain point, further increase in the depth does not lead to significant cooling of the PV. The results show that, for $\Sigma I_T = 3$ kWh/m^2/day, the increase in the depth beyond 2.4 cm cannot lead to the decrement in the PV temperature more than 1 °C. Thus, 2.4 cm depth can be considered as the best for $\Sigma I_T = 3$ kWh/m^2/day. It must be noted that, for the values of I_T lesser than 400 W/m^2, the rate of heat extraction by PCM is very less. Thus, while summing up the values of I_T over a day for obtaining ΣI_T, the values of I_T larger than 400 W/m^2 should only be considered.

5.1. Effect of wind azimuth angle

For different daily solar radiation levels, the effect of wind azimuth angle (γ) on the optimum depth of the PCM container is presented in Fig. 5. It has been observed that with increase in the wind azimuth angle, the optimum depth increases. For lesser wind azimuth angles, the wind flows almost normal to the surface causing greater heat losses due to forced convection. For the larger wind azimuth angles, the heat losses are lesser leading to higher rate of heat extraction by PCM. Due to this, the PCM melts in shorter duration as can be seen from Fig. 6. Thus, for larger wind azimuth angles, larger quantities of PCM are required to keep the PV cooler.

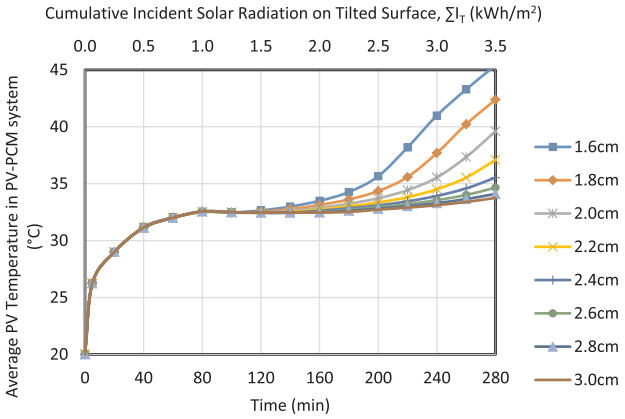

Fig. 4. Variation in the average temperature of PV (in PV-PCM system) with time for various depths of PCM container.

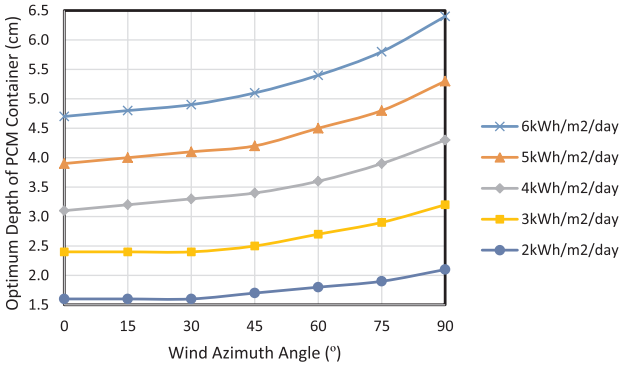

Fig. 5. Variation in the optimum depth of PCM container with wind azimuth angle (γ) for various solar radiation levels (ΣI_T).

5.2. Effect of wind velocity

Fig. 7 shows the variation in the optimum depth of the PCM container against different values of wind velocities (v_w) at various daily solar radiation values. It is observed that the optimum depth decreases as wind velocity increases. For lower wind velocities, the heat losses are lesser which cause higher rate of heat extraction by PCM resulting in its quick melting as evident from Fig. 8. Thus, larger quantity of PCM is required to cool the PV for desired duration for lesser wind velocities.

Table 2
Thermal properties of PCM (RT 25 HC) and values of other parameters used for calculations.

Parameter	Value	Parameter	Value	Parameter	Value	Parameter	Value
C_p (J/kg K)	1800/2400 (solid/liquid phase)	T_a (°C)	20	β_c (K^{-1})	0.001	$\eta_{PV\ module}$ (%)	20[1 − 0.005(T_{PV} − 25) + 0.085 ln (I_T/1000)]
I_T (W/m^2)	750	T_m (°C)	26.6	γ (°)	0	μ (kg/m s)	10^5/0.001798
k (W/m K)	0.19/0.18	v_w (m/s)	4	ΔT (°C)	2	ρ (kg/m^3)	785
L_h (J/kg)	232,000	β (°)	45	ε	0.85	ρ_{PV}	0.1

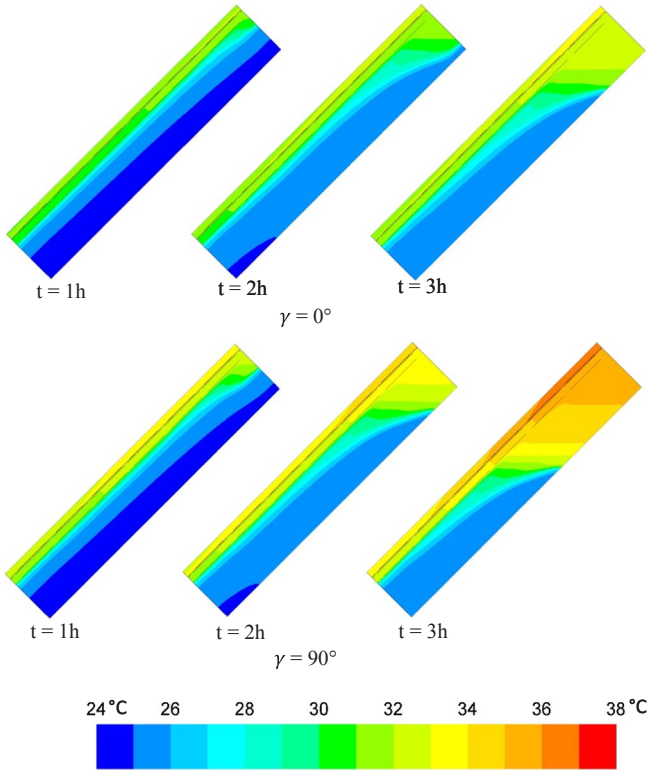

Fig. 6. Variation in the temperature of PV-PCM system with time for different values of wind azimuth angle (γ) keeping δ = 3 cm.

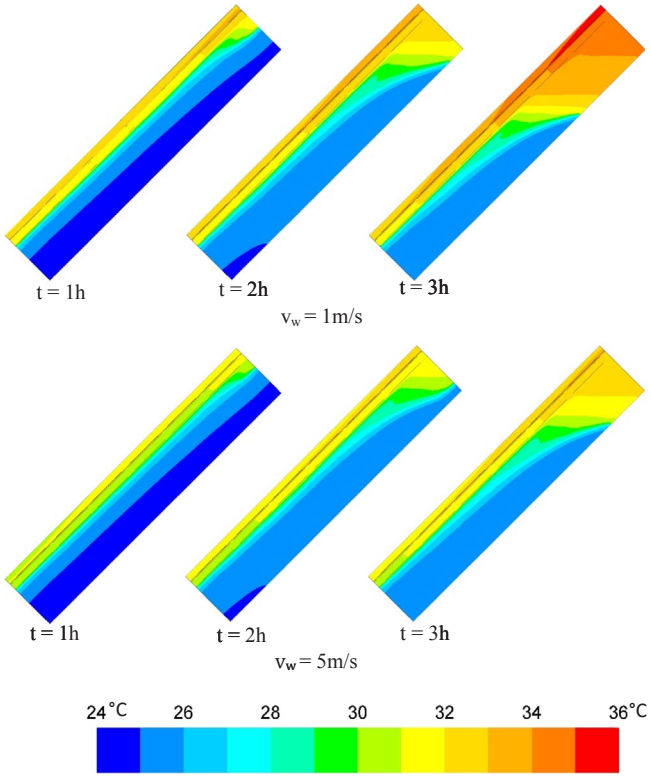

Fig. 8. Variation in the temperature of PV-PCM system with time for different values of wind velocity (v_w) keeping δ = 3 cm.

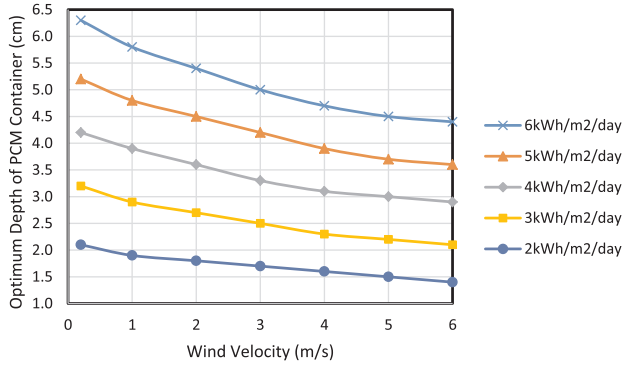

Fig. 7. Variation in the optimum depth of PCM container with wind velocity (v_w) for various solar radiation levels (ΣI_T).

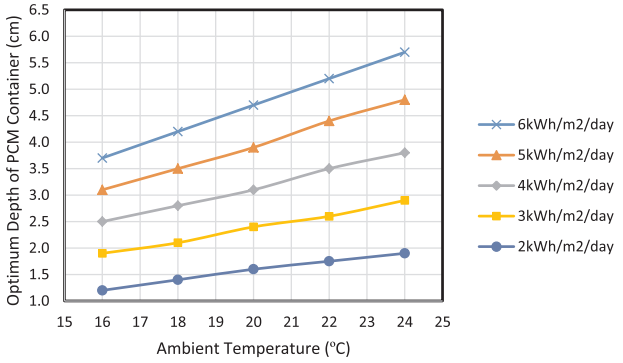

Fig. 9. Variation in the optimum depth of PCM container with ambient temperature (T_a) for various solar radiation levels (ΣI_T).

5.3. Effect of ambient temperature

The optimum depths of the PCM container were calculated for various values of the ambient temperature (T_a) at different daily solar radiation levels and are presented in Fig. 9. The results show that with rise in the ambient temperature, the optimum depth increases. Higher ambient temperatures lead to lesser heat losses causing heat extraction by PCM at higher pace. It results in early melting of the PCM as shown in Fig. 10. Thus, for higher ambient temperature, more quantity of the PCM is required to cool the PV during operation.

5.4. Effect of melting temperature of PCM

The optimum depths of the PCM container for different melting temperatures of the PCM (T_m) are shown in Fig. 11 for various combinations of the ambient temperature and the wind velocity. For this, different PCMs (RT 35 HC, RT 28 HC and RT 22 HC (Rubitherm Phase Change Material, 2017) were chosen. The results show that the lower T_m leads to higher optimum depth. The PCM with lesser melting temperature (near to ambient) can maintain the PV at lower temperature which results in lesser heat losses from the system and, thus, higher rate of heat extraction by the PCM. Thus, for lower T_m, the PCM melts in shorter duration and larger quantity of the PCM is required to cool the PV during the entire operation. It must also be noted that the lesser latent heat capacity also leads to the requirement of larger PCM quantity to cool the PV.

For sunny seasons at Cornwall UK (50.17°N, 5.12°W), the ambient temperature remains near to 18 °C during sunshine hours. Thus, RT 22 HC PCM can be used. The average ΣI_T is around 4.2 kWh/m^2/day with high wind velocity. Thus, Fig. 11 shows that 4.1 cm is the optimum depth of the PCM container.

A summary of the results have been presented in Table 3. The results show that the ambient temperature affects the melting of the PCM/optimum depth the most.

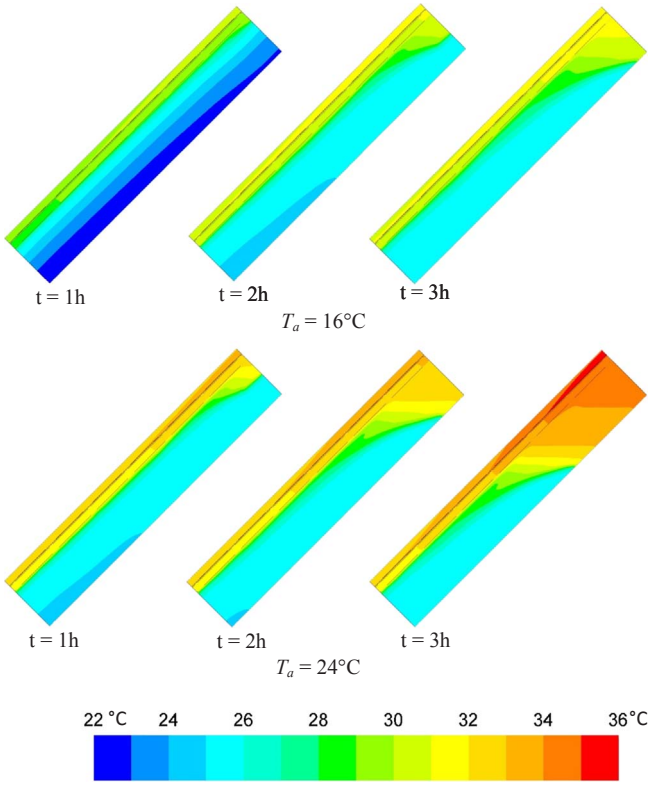

Fig. 10. Variation in the temperature of PV-PCM system with time for different values of ambient temperature (T_a) keeping $\delta = 3$ cm.

6. Conclusions

A mathematical model has been presented for analysing the thermal performance of the PV-PCM system. Heat transfer due to conduction, convection and radiation were accounted. In order to validate the model, the temperature variations in the system with time had been computed and compared with the established results. The differences of the calculated values from the reported numerical and experimental ones lie within -1.5 °C to $+1.5$ °C and -2.0 °C to $+0.7$ °C respectively. It is also observed that once the PCM is fully melted, the PV temperature starts increasing rapidly with time. By increasing the quantity of the PCM (i.e. the depth of the PCM container), the duration can be increased for which the PV can be maintained at lower temperature. For the presented work, the variations in the temperature of the PV-PCM system with time had been computed for various depths of the PCM container and the optimum depth of container was calculated for various daily solar radiation levels. The effect of operating conditions viz. wind velocity, wind azimuth angle i.e. wind direction, ambient temperature and melting temperature of the PCM on the optimum PCM quantity had also been analysed. It can be concluded from the results that

(i) As wind velocity increases from 1 m/s to 5 m/s, optimum depth of PCM container decreases from 4.8 cm to 3.7 cm for $\Sigma I_T = 5$ kWh/m^2/day and from 2.9 cm to 2.2 cm for $\Sigma I_T = 3$ kWh/m^2/day.
(ii) Wind azimuth angle has no significant effect on the system's performance if wind velocity is very low. Otherwise, as wind azimuth angle increases from 0° to 90°, optimum depth of PCM container increases from 3.9 cm to 5.3 cm for $\Sigma I_T = 5$ kWh/m^2/day and from 2.4 cm to 3.2 cm for $\Sigma I_T = 3$ kWh/m^2/day.
(iii) As ambient temperature increases from 16 °C to 24 °C, optimum depth of PCM container increases from 3.1 cm to 4.8 cm for $\Sigma I_T = 5$ kWh/m^2/day and from 1.9 cm to 2.9 cm for $\Sigma I_T = 3$ kWh/m^2/day.

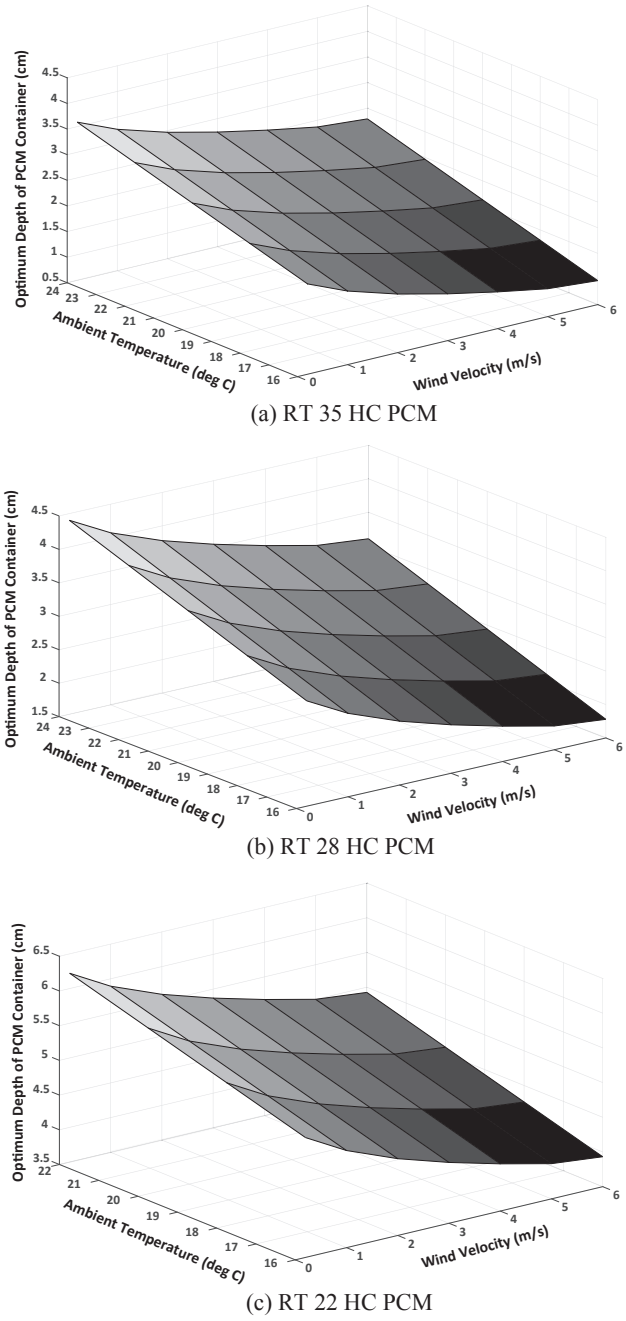

Fig. 11. Variation in the optimum depth of PCM container for various PCMs for $\Sigma I_T = 4$ kWh/m^2/day.

Table 3
Optimum depths of PCM container for various values of ambient temperature (T_a), wind azimuth angle (γ), wind velocity (v_w) for RT 25 HC PCM and $\Sigma I_T = 6$ kWh/m^2/day.

T_a (°C)	Optimum depth (cm)	γ (°)	Optimum depth (cm)	v_w (m/s)	Optimum depth (cm)
12	2.6	0	4.7	0.2	6.3
14	3.2	15	4.8	1	5.8
16	3.7	30	4.9	2	5.4
18	4.2	45	5.1	3	5.0
20	4.7	60	5.4	4	4.7
22	5.2	75	5.8	5	4.5
24	5.7	90	6.4	6	4.4

(iv) The PCM having lower melting temperature (near to ambient) can maintain the PV at lower temperature but needs larger PCM quantity for PV cooling. It must also be noted that the lesser latent heat capacity also leads to the requirement of larger PCM quantity.

It must be mentioned that (i) the presented model considers a perfect contact between the PV rear and the PCM container. However, it is tough to achieve which slightly reduces the rate of heat extraction by the PCM container and, consequently, decreases the optimum depth. (ii) the presented model considers the perfect solidification of the PCM. However, Huang et al. (2011) reported that the solidification leaves voids inside the PCM. It will reduce the rate of heat extraction by the PCM and decrease the optimum depth.

Acknowledgment

The authors gratefully acknowledge the financial support from EPSRC-DST funded Reliable and Efficient System for Community Energy Solution - RESCUES project (EP/K03619X/1). In support of open access research, all underlying article materials (such as data, samples or models) can be accessed upon request via email to the corresponding author.

References

Aelenei, L., Pereira, R., Gonçalves, H., Athienitis, A., 2014. Thermal performance of a hybrid BIPV-PCM: modeling, design and experimental investigation. Energy Proc. 48, 474–483.
Atkin, P., Farid, M.M., 2015. Improving the efficiency of photovoltaic cells using PCM infused graphite and aluminium fins. Sol. Energy 114, 217–228.
Biwole, P.H., Eclache, P., Kuznik, F., 2013. Phase-change materials to improve solar panel's performance. Energy Build. 62, 59–67.
Brano, V.L., Ciulla, G., Piacentino, A., Cardona, F., 2014. Finite difference thermal model of a latent heat storage system coupled with a photovoltaic device: description and experimental validation. Renew. Energy 68, 181–193.
Browne, M.C., Norton, B., McCormack, S.J., 2015a. Phase change materials for photovoltaic thermal management. Renew. Sustain. Energy Rev. 47, 762–782.
Browne, M.C., Lawlor, K., Kelly, A., Norton, B., McCormack, S.J., 2015b. Indoor characterisation of a photovoltaic/ thermal phase change material system. Energy Proc. 70, 163–171.
Browne, M.C., Quigley, D., Hard, H.R., Gilligan, S., Ribeiro, N.C.C., Almeida, N., McCormack, S.J., 2016. Assessing the thermal performance of phase change material in a photovoltaic/thermal system. Energy Proc. 91, 113–121.
Du, D., Darkwa, J., Kokogiannakis, G., 2013. Thermal management systems for Photovoltaics (PV) installations: a critical review. Sol. Energy 97, 238–254.
Elarga, H., Goia, F., Zarrella, A., Monte, A.D., Benini, E., 2016. Thermal and electrical performance of an integrated PV-PCM system in double skin façades: a numerical study. Sol. Energy 136, 112–124.
Emam, M., Ookawara, S., Ahmed, M., 2017. Performance study and analysis of an inclined concentrated photovoltaic-phase change material system. Sol. Energy 150, 229–245.
Hasan, A., McCormack, S.J., Huang, M.J., Norton, B., 2010. Evaluation of phase change materials for thermal regulation enhancement of building integrated photovoltaics. Sol. Energy 84, 1601–1612.
Hasan, A., McCormack, S.J., Huang, M.J., Sarwar, J., Norton, B., 2015. Increased photovoltaic performance through temperature regulation by phase change materials: materials comparison in different climates. Sol. Energy 115, 264–276.
Ho, C.J., Tanuwijava, A.O., Lai, C.M., 2012. Thermal and electrical performance of a BIPV integrated with a microencapsulated phase change material layer. Energy Build. 50, 331–338.
Ho, C.J., Chou, W.L., Lai, C.M., 2014. Application of a water-saturated MEPCM-PV for reducing winter chilling damage on aqua farms. Sol. Energy 108, 135–145.
Ho, C.J., Chou, W.L., Lai, C.M., 2015. Thermal and electrical performance of a water-surface floating PV integrated with a water-saturated MEPCM layer. Energy Convers. Manage. 89, 862–872.
Huang, M.J., 2011. The effect of using two PCMs on the thermal regulation performance of BIPV systems. Sol. Energy Mater. Sol. Cells 95, 957–963.
Huang, M.J., Eames, P.C., Norton, B., 2004. Thermal regulation of building-integrated photovoltaics using phase change materials. Int. J. Heat Mass Transf. 47, 2715–2733.
Huang, M.J., Eames, P.C., Norton, B., 2006a. Phase change materials for limiting temperature rise in building integrated photovoltaics. Sol. Energy 80, 1121–1130.
Huang, M.J., Eames, P.C., Norton, B., 2006b. Comparison of a small-scale 3D PCM thermal control model with a validated 2D PCM thermal control model. Sol. Energy Mater. Sol. Cells 90, 1961–1972.
Huang, M.J., Eames, P.C., Norton, B., 2007. Comparison of predictions made using a new 3D phase change material thermal control model with experimental measurements and predictions made using a validated 2D model. Heat Transfer Eng. 28, 31–37.
Huang, M.J., Eames, P.C., Norton, B., Hewitt, N.J., 2011. Natural convection in an internally finned phase change material heat sink for the thermal management of photovoltaics. Sol. Energy Mater. Sol. Cells 95, 1598–1603.
Indartono, Y.S., Suwono, A., Pratama, F.Y., 2014. Improving photovoltaics performance by using yellow petroleum jelly as phase change material. Int. J. Low-Carbon Technol. 1–5.
Kant, K., Shukla, A., Sharma, A., Biwole, P.H., 2016. Heat transfer studies of photovoltaic panel coupled with phase change material. Sol. Energy 140, 151–161.
Kaplani, E., Kaplanis, S., 2014. Thermal modelling and experimental assessment of the dependence of PV module temperature on wind velocity and direction, module orientation and inclination. Sol. Energy 107, 443–460.
Khanna, S., Sundaram, S., Reddy, K.S., Mallick, T.K., 2017a. Performance analysis of perovskite and dye-sensitized solar cells under varying operating conditions and comparison with monocrystalline silicon cell. Appl. Therm. Eng. 127, 559–565.
Khanna, S., Reddy, K.S., Mallick, T.K., 2017b. Performance analysis of tilted photovoltaic system integrated with phase change material. Energy 133, 887–899.
Kibria, M.A., Saidur, R., Al-Sulaiman, F.A., Aziz, M.M.A., 2016. Development of a thermal model for a hybrid photovoltaic module and phase change materials storage integrated in buildings. Sol. Energy 124, 114–123.
Ma, T., Yang, H., Zhang, Y., Lu, L., Wang, X., 2015. Using phase change materials in photovoltaic systems for thermal regulation and electrical efficiency improvement: a review and outlook. Renew. Sustain. Energy Rev. 43, 1273–1284.
Mahamudul, H., Rahman, M.M., Metselaar, H.S.C., Mekhilef, S., Shezan, S.A., Sohel, R., Karim, S.B.A., Badiuzaman, W.N.I., 2016. Temperature regulation of photovoltaic module using phase change material: a numerical analysis and experimental investigation. Int. J. Photoenergy 5917028, 1–8.
Park, J., Kim, T., Leigh, S.B., 2014. Application of a phase-change material to improve the electrical performance of vertical-building-added photovoltaics considering the annual weather conditions. Sol. Energy 105, 561–674.
Rubitherm Phase Change Material <https://www.rubitherm.eu/> (accessed 20.07. 2017).
Sharma, S., Tahir, A., Reddy, K.S., Mallick, T.K., 2016. Performance enhancement of a building-integrated concentrating photovoltaic system using phase change material. Sol. Energy Mater. Sol. Cells 149, 29–39.
Shukla, A., Kant, K., Sharma, A., Biwole, P.H., 2017. Cooling methodologies of photovoltaic module for enhancing electrical efficiency: a review. Sol. Energy Mater. Sol. Cells 160, 275–286.
Smith, C.J., Forster, P.M., Crook, R., 2014. Global analysis of photovoltaic energy output enhanced by phase change material cooling. Appl. Energy 126, 21–28.